# Supplementary information for 'Assessing model predictions of carbon dynamics in global drylands' by Fawcett and Cunliffe et al.
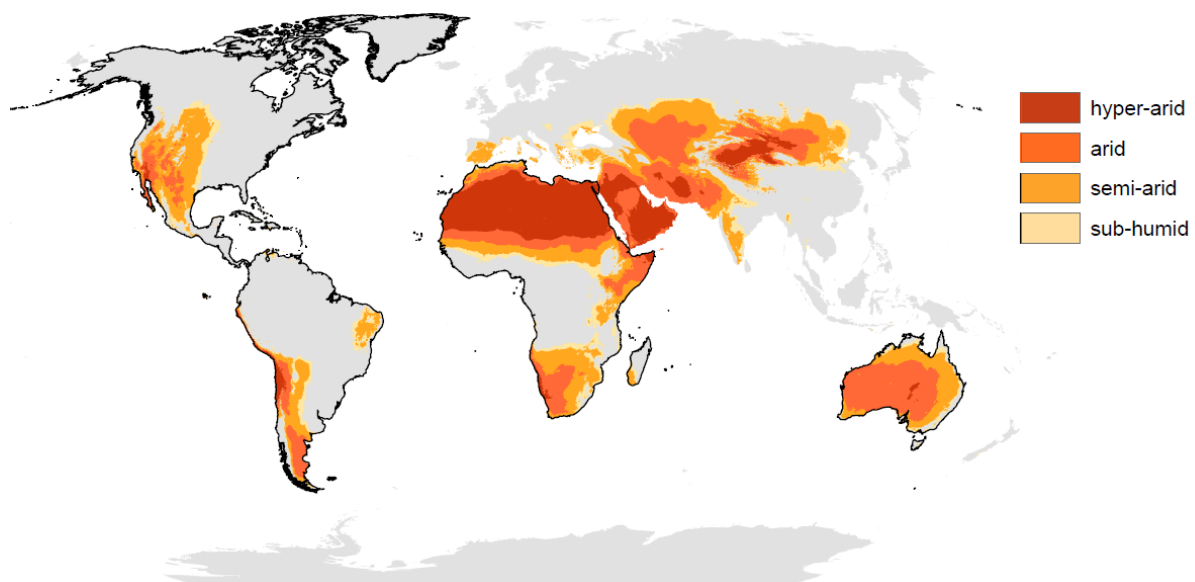


Fig. S1. Distribution of global drylands defined by the aridity index, the ratio of precipitation to potential evapotranspiration based on 1981-2010 mean gridded surface climatology (TerraClimate). We classified drylands as one of the four following climate classes: Hyper-arid: $P/PET < 0.05$, Arid: $0.05 < P/PET < 0.2$, Semi-arid: $0.2 < P/PET < 0.5$, Sub-humid: $0.5 < P/PET < 0.65$. We masked areas north and south of 55 degrees from the Equator, to exclude high-latitude arid permafrost areas. Bold outlines indicate the continent regions where AGC could be compared to L-VOD-based estimates and oceans are masked in all figures.
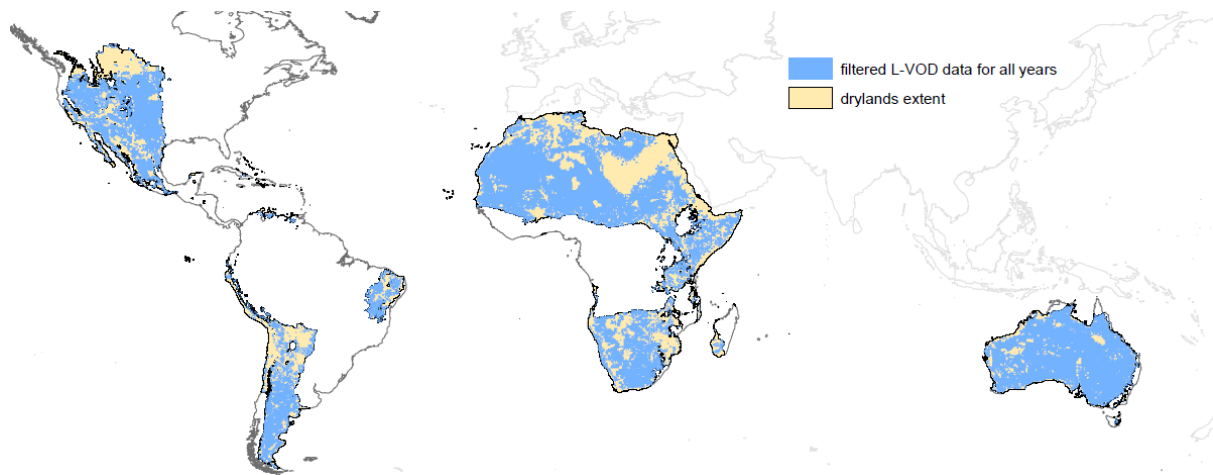
Fig. S2. Global map depicting dryland areas with retained L-VOD observations after quality filtering for the full period (2011-2018) that were used for the temporal analysis of above ground carbon. These areas covered ca. 64% of the total dryland areas for these continents (Figure S1).
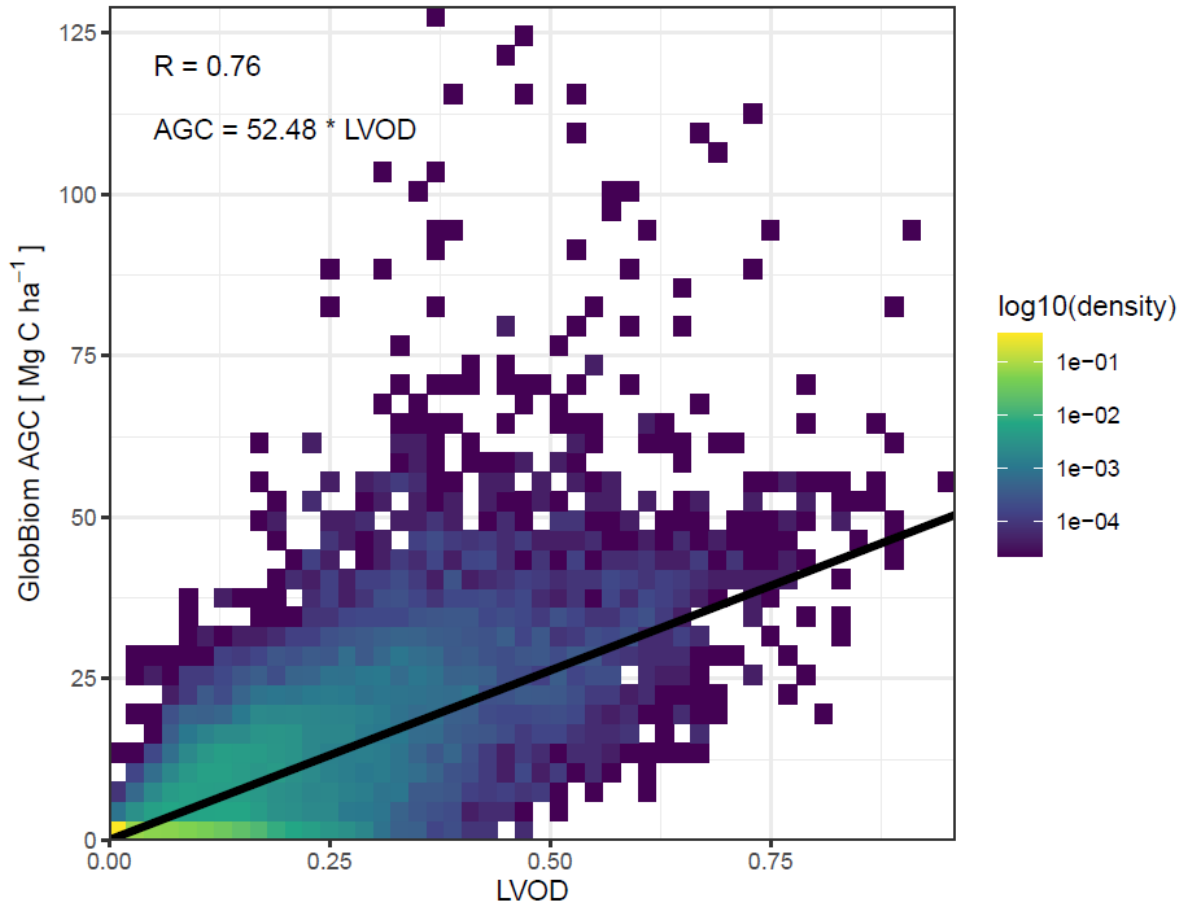
Fig. S3. We used the biomass map (GlobBiomass, Santoro et al., 2018) with the best correlation to L-VOD for global drylands to develop a new, drylands-specific biomass transfer function relating L-VOD to aboveground carbon. It was necessary to develop a drylands-specific biomass transfer function because previous linear models (e.g. Brandt et al. 2018) calibrated against data including high-biomass ecosystems like tropical forests tend to overestimate dryland biomass. It should be noted that intercomparisons reveal disagreements remaining between different biomass products in savannas and sparsely vegetated shrublands and grasslands (Zhang et al., 2019b) and there is clearly room for improvement in biomass data used for this calibration. We constrained the intercept through zero because areas with zero biomass have zero L-VOD (Brandt et al. 2018). The resulting linear model relating L-VOD to AGC has a slope of 52.48 (95% CI: 52.12-52.84) [Mg C ha$^{-1}$], standard error = 0.18 and $R^2$ = 0.65.
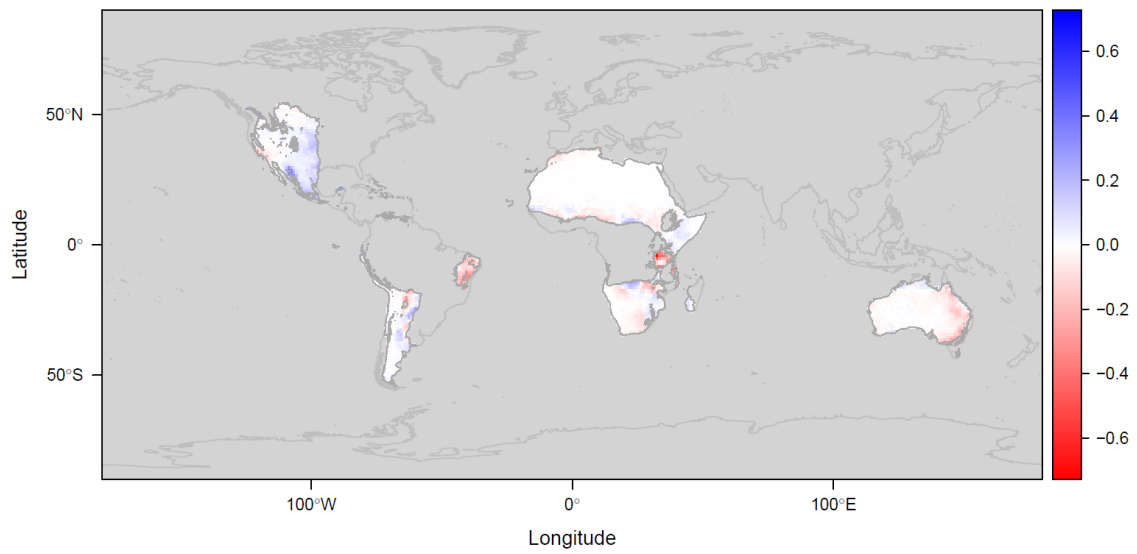
**a) L−VOD**
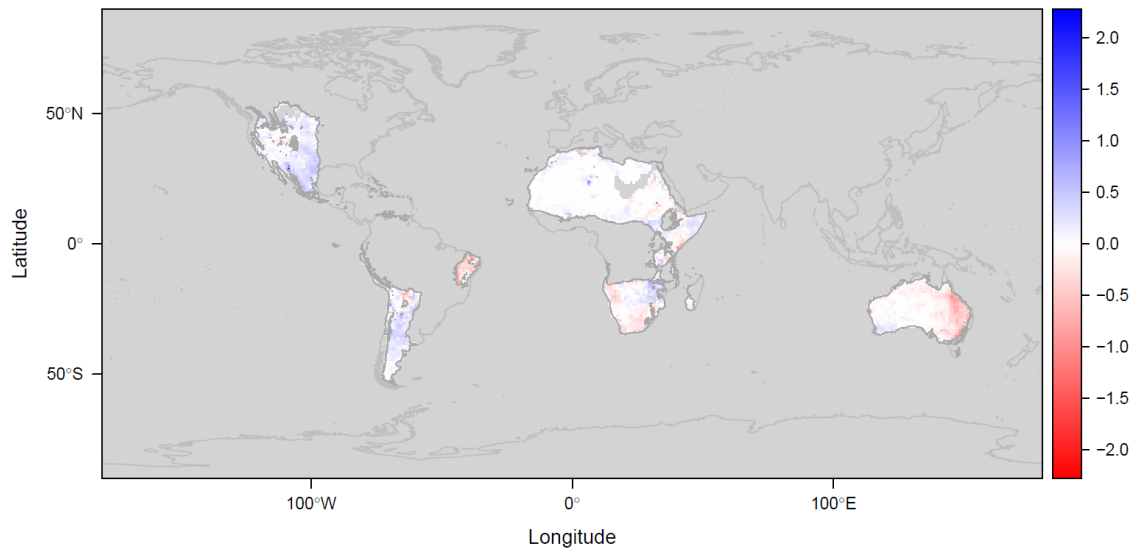


**b) TRENDY−mean**



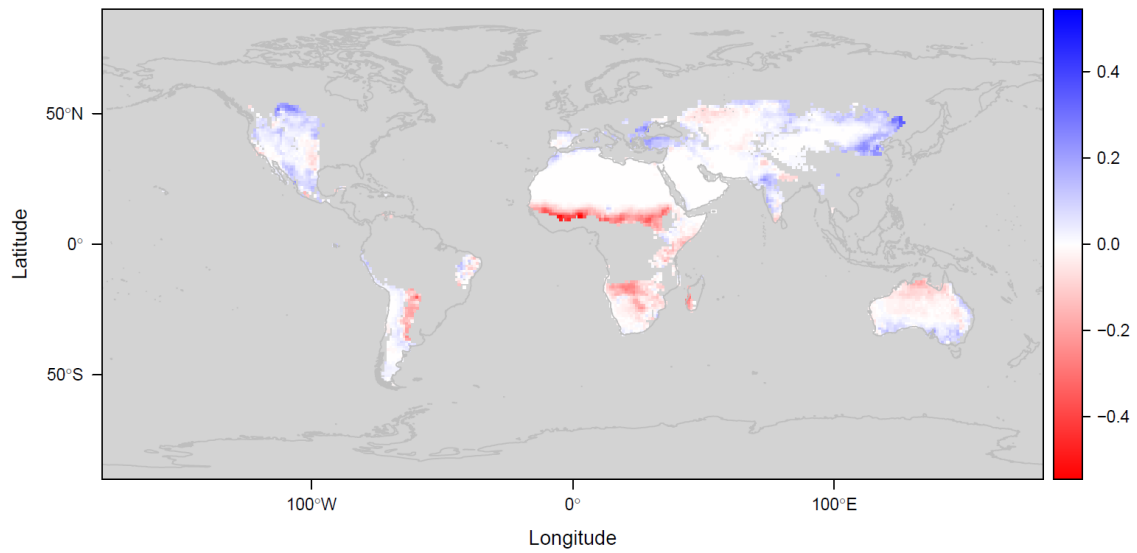Fig. S4. Maps of trends (2011-2018) in AGC for climatic drylands of the studied continents with reliable L-VOD data. Units are Mg C ha$^{-1}$ yr$^{-1}$.

**a) MODIS PML-v2**



**b) TRENDY-mean**
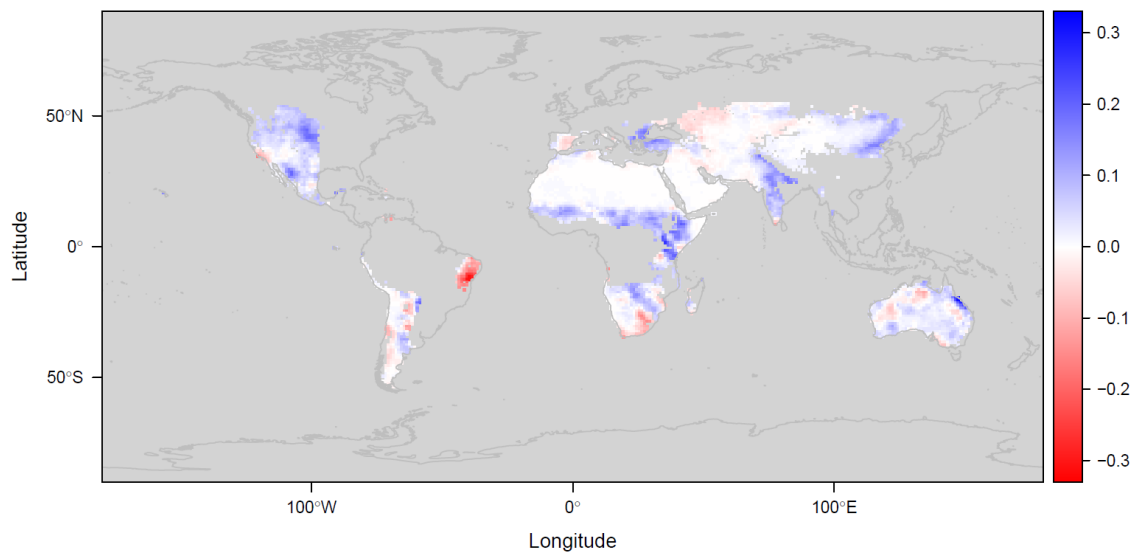


Fig. S5: Maps of trends (2001-2018) in GPP for global climatic drylands. Units are Mg C ha$^{-1}$ yr$^{-1}$.

Fig. S6: Difference between productivity (mean GPP 2001-2018) derived from MODIS observations and simulations by the TRENDY models over global drylands (TRENDY model - MODIS GPP). Units are Mg C ha^{-1} yr^{-1}.

43

Model − MODIS PML−v2 annual GPP trend  [ Mg C ha$^{-1}$ yr$^{-1}$ ]
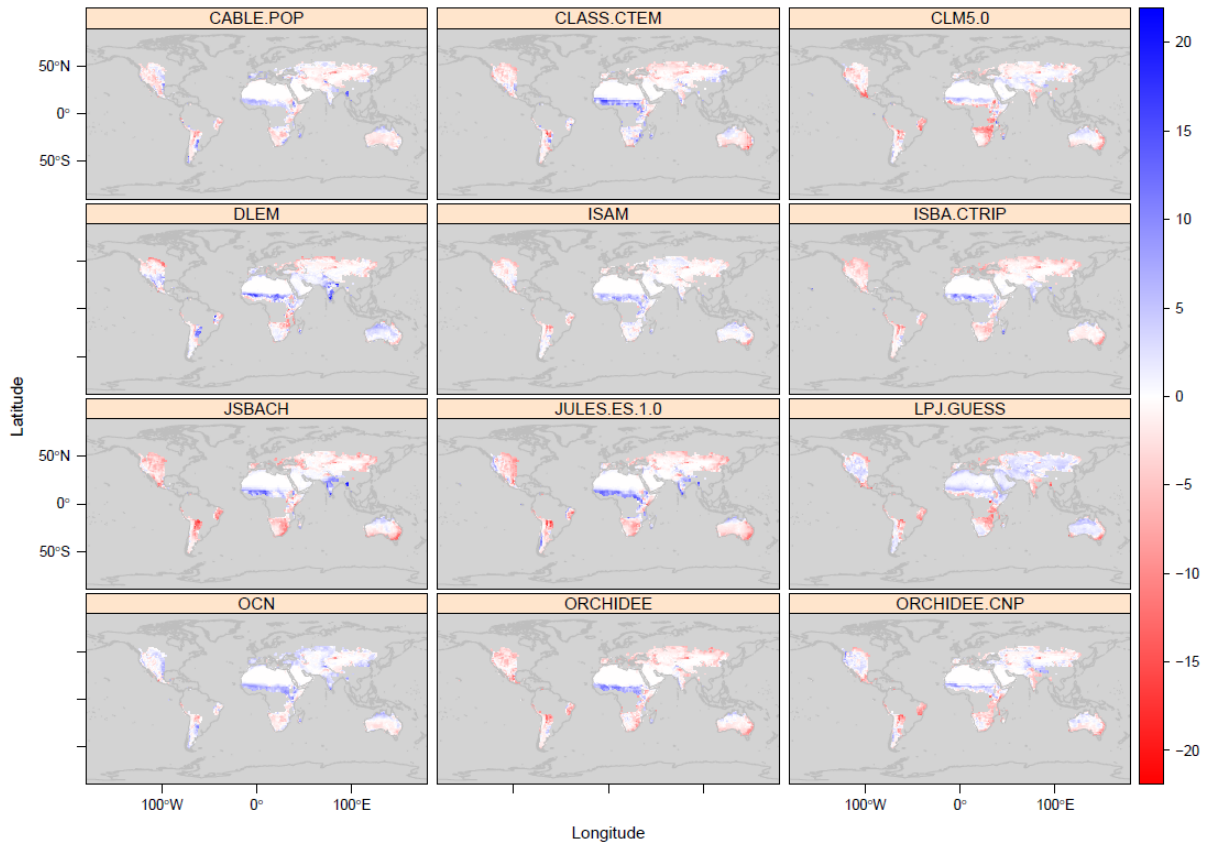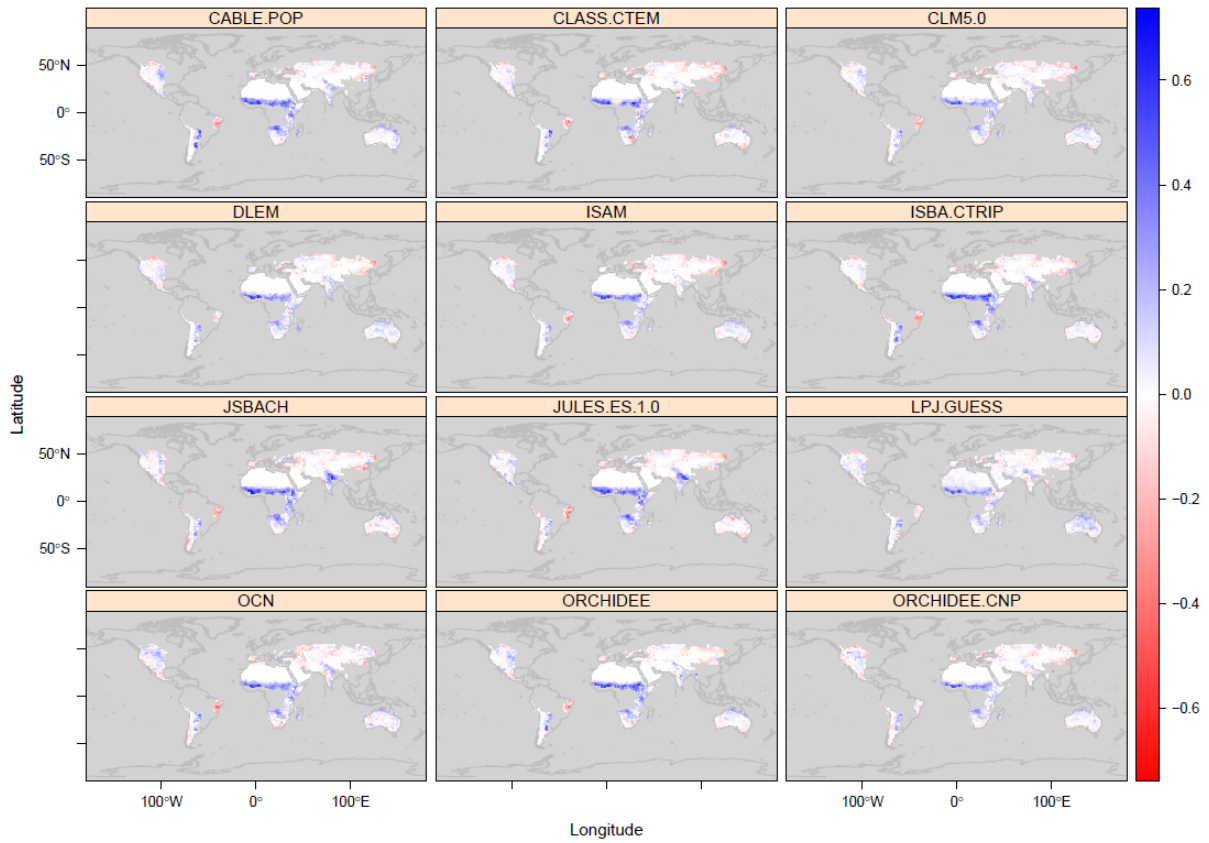


Fig. S7: Difference between productivity trends (annual GPP 2001-2018) derived from MODIS observations and simulations by the TRENDY models over global drylands (TRENDY model - MODIS GPP). Units are Mg C ha$^{-1}$ yr$^{-1}$.
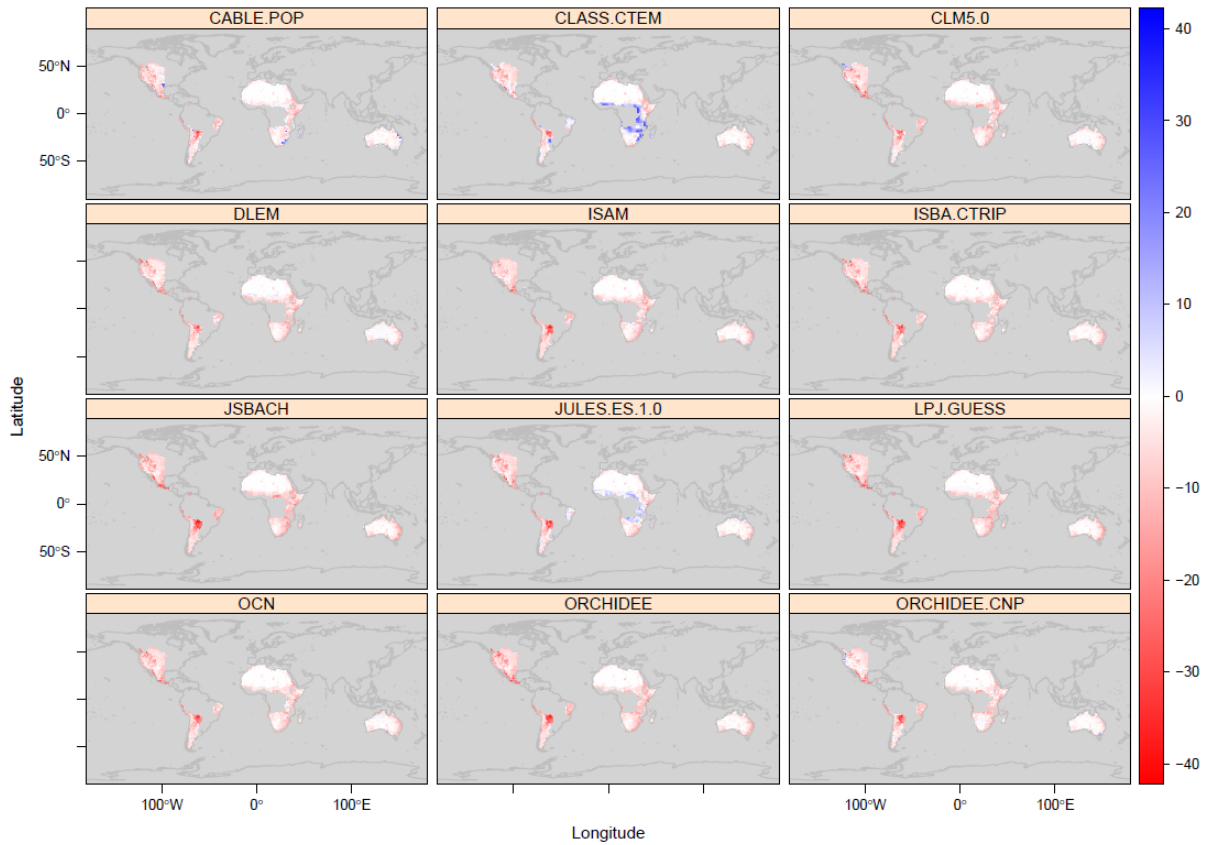
Fig. S8: Difference between AGC (mean 2011-2018) inferred from L-VOD and simulated by the TRENDY models for climatic drylands of the studied continents with reliable L-VOD data (TRENDY model - L-VOD AGC). Units are Mg C ha$^{-1}$.
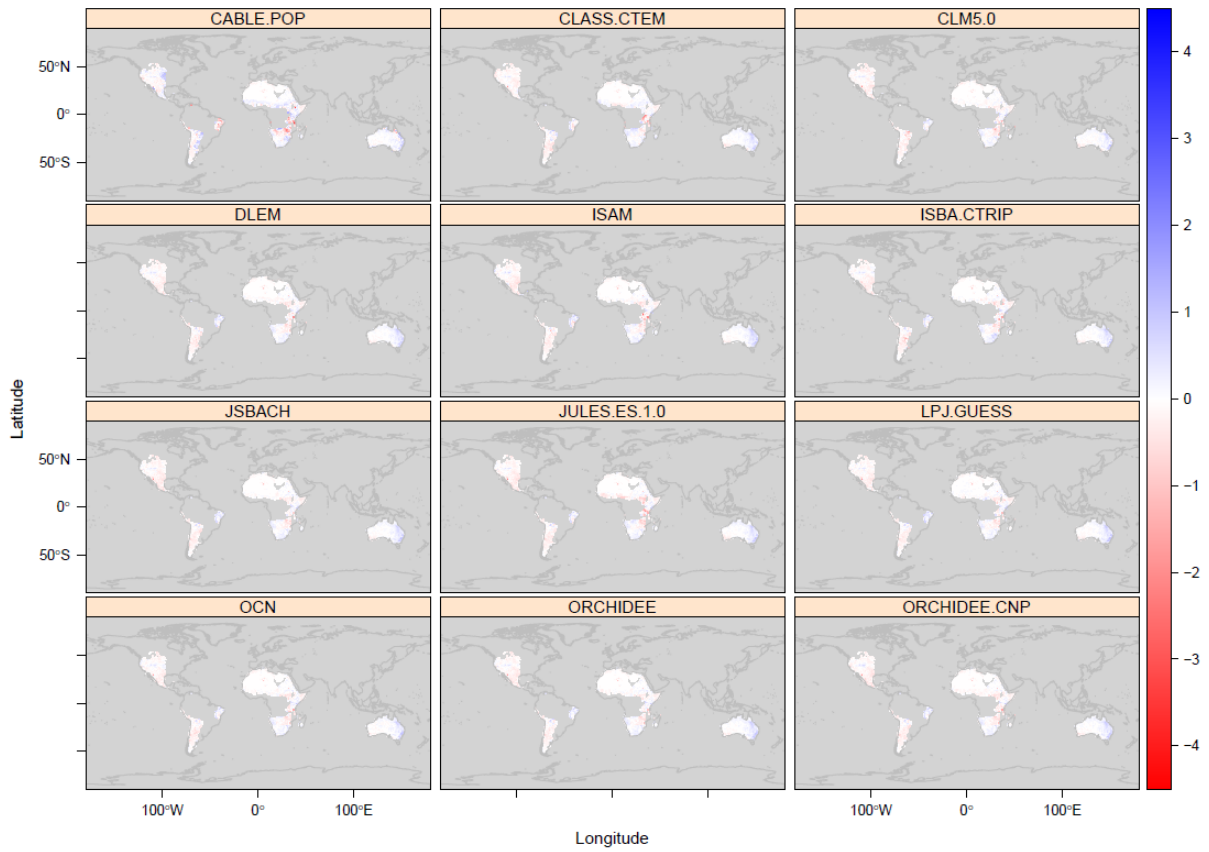
Fig. S9: Difference between AGC trends (2011-2018) inferred from L-VOD and simulated by the TRENDY LSMs for climatic drylands of the studied continents with reliable L-VOD data (TRENDY model - L-VOD AGC). Units are Mg C ha$^{-1}$ yr$^{-1}$.

burned frequency 2001−2018
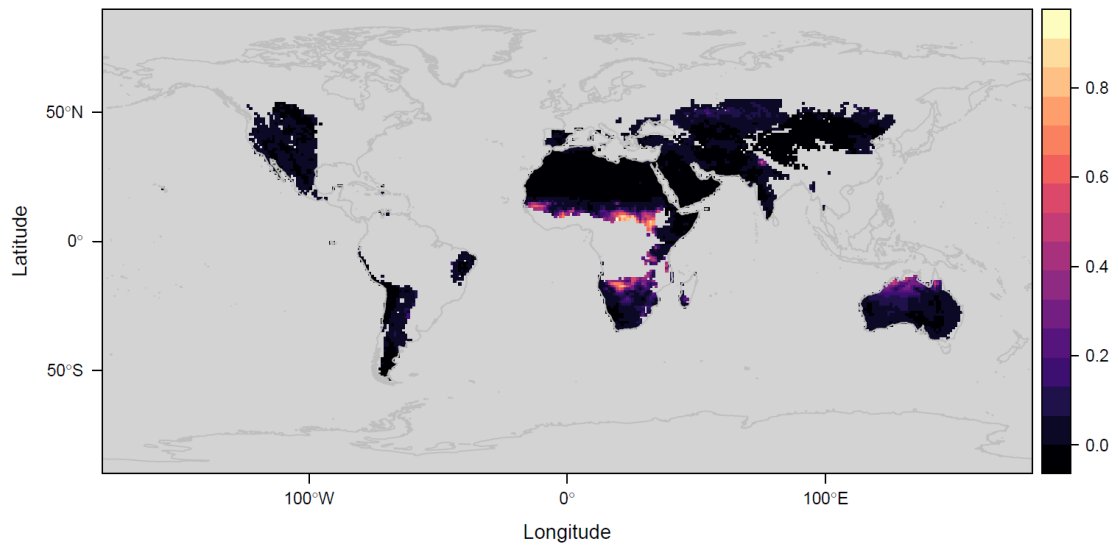


Fig. S10: Frequency of burned area between 2001-2018, extracted from the MCD64A1v006 burned area product and resampled to 1° gridcell. Values of 0.5 might indicate the entire pixel burned every two years or that half the pixel burned every year.
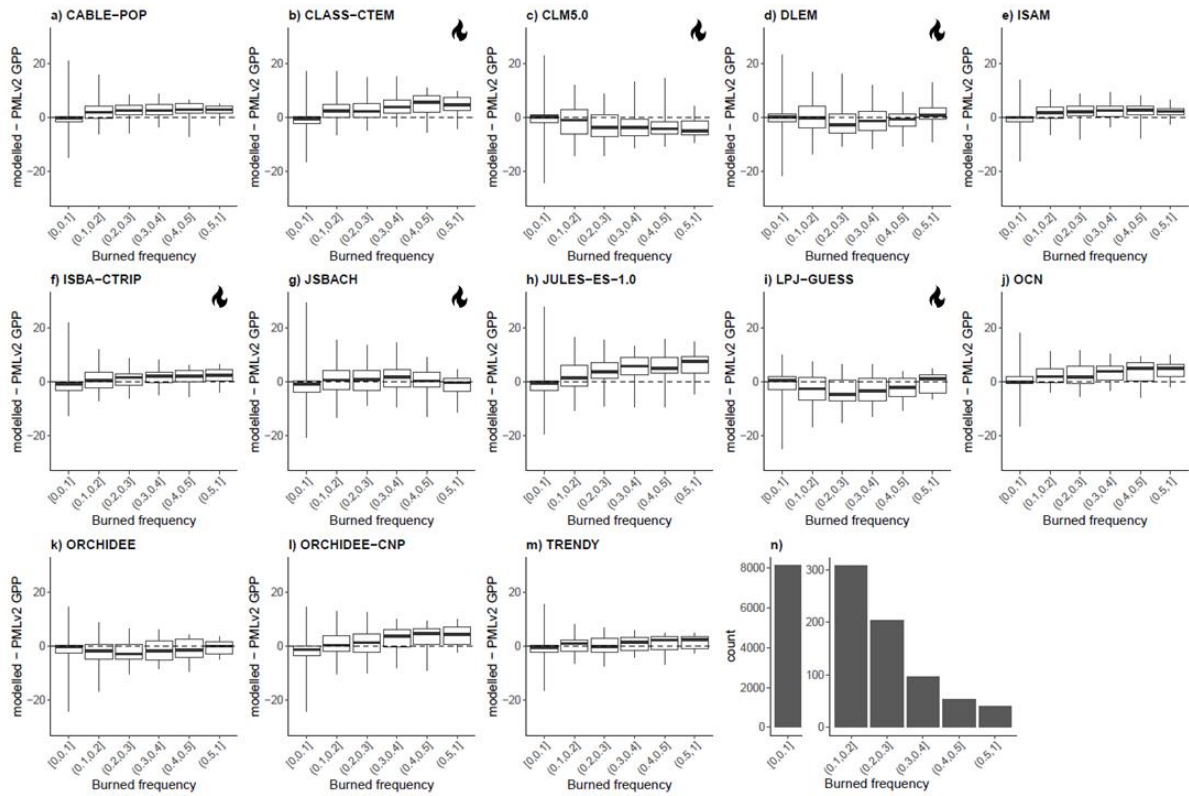
Fig. S11. GPP model-data comparison for different fire frequencies. Units are GPP (Mg C ha$^{-1}$ y$^{-1}$). We saw little systematic relationship between burn frequency and GPP bias, although some models (JULES and CLASS-CTEM, ORCHIDEE-CNP, and OCN) did overestimate GPP in more frequently burned areas. Models with explicit representation of fire are indicated by the black flame icon. Black lines are the medians, rectangles are interquartile range and whiskers extend from maximum to minimum. The histogram (n) indicates the number of grid-cells per burned frequency bin.
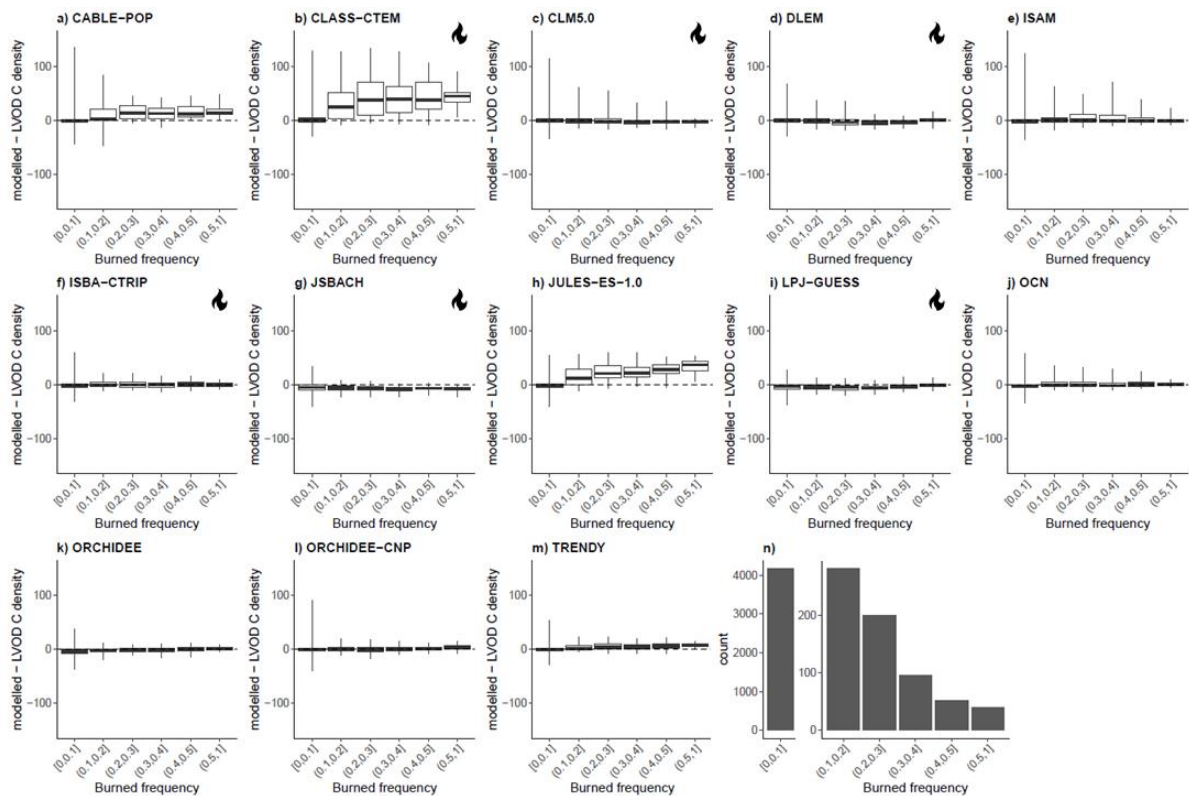
Fig. S12. AGC model-data comparison for different fire frequencies. Units are AGC density (Mg C ha⁻¹). There was generally no relation between burn frequency and model - data residuals, apart from JULES and CLASS-CTEM which overestimated biomass in more frequently burned regions. Models with explicit representation of fire are indicated by the black flame icon. Black lines are the medians, rectangles are interquartile range and whiskers extend from maximum to minimum. The histogram (n) indicates the number of grid-cells per burned frequency bin.

Fig. S13: Effects of a) CO2 increase, b) climate change, c) land-use change and d) combined on cVeg, using TRENDY model runs S1: changing CO2 and recycled climatology, S2: changing CO2 and varying climatology and S3: changing CO2, varying climatology and land-use change. (d-f) show the model means with ribbons representing the interquartile range. The divergence is shown relative to 1901. The model set used to generate this figure is identical to Fig. 6.
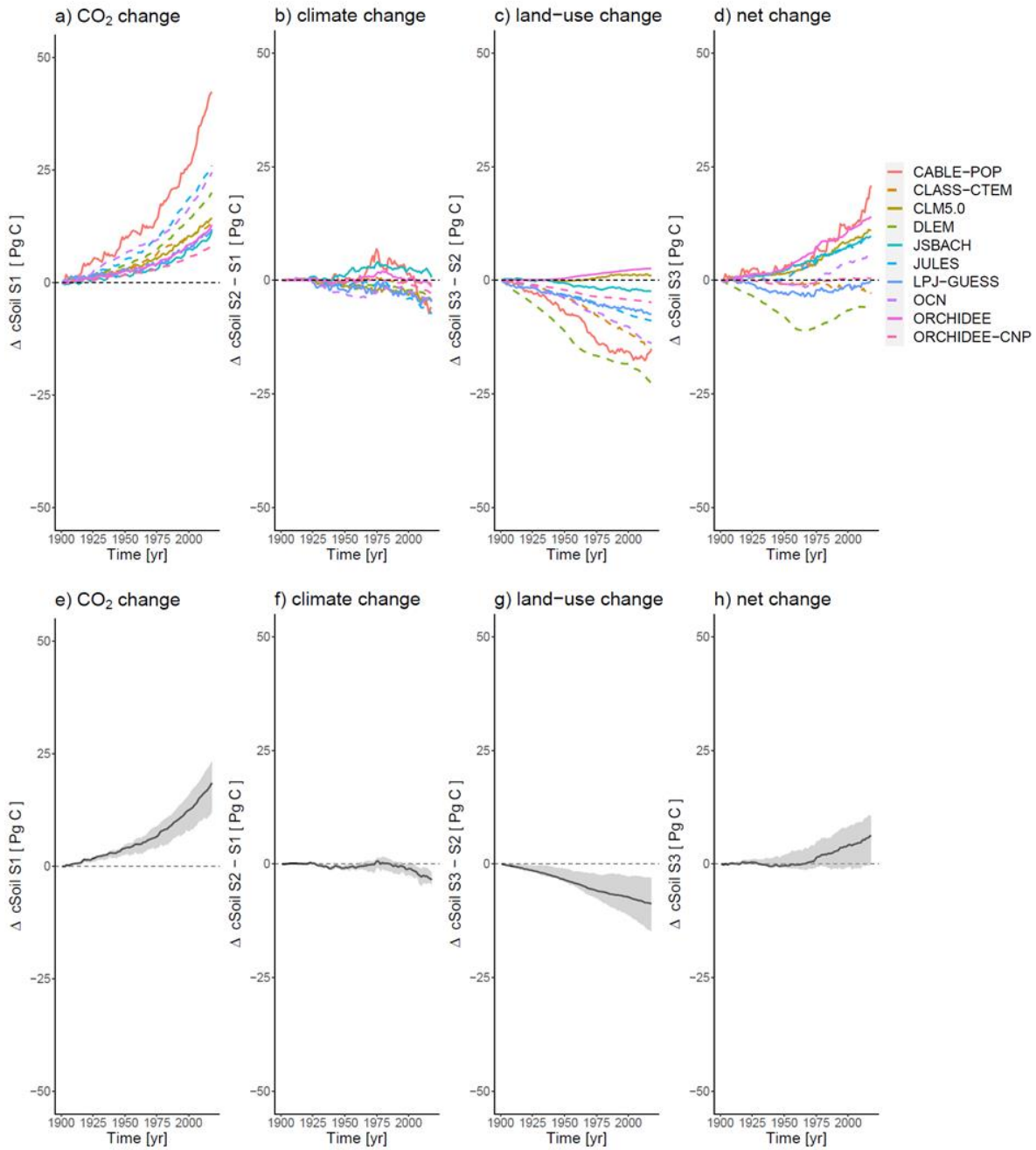
Fig. S14: Effects of a) CO2 increase, b) climate change, c) land-use change and d) combined on cSoil, using TRENDY model runs S1: changing CO2 and recycled climatology, S2: changing CO2 and varying climatology and S3: changing CO2, varying climatology and land use change. (d-f) show the model means with ribbons representing the interquartile range. The divergence is shown relative to 1901. The model set used to generate this figure excludes ISAM as an S1 run for cSoil was not available.
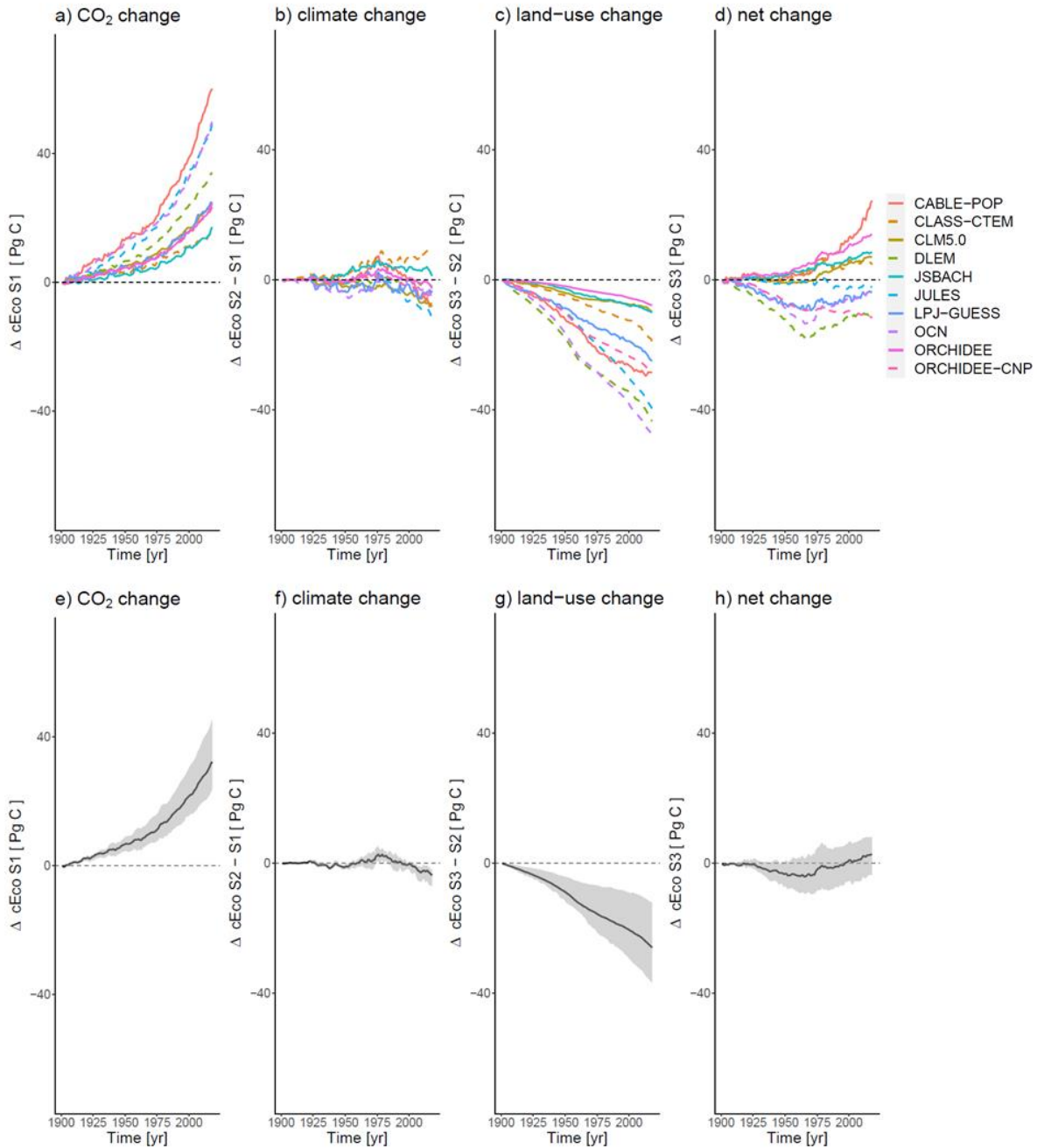
Fig. S15: Effects of a) CO2 increase, b) climate change, c) land-use change and d) combined on cEco, using TRENDY model runs S1: changing CO2 and recycled climatology, S2: changing CO2 and varying climatology and S3: changing CO2, varying climatology and land-use change. (d-f) show the model means with ribbons representing the interquartile range. The divergence is shown relative to 1901. The model set used to generate this figure excludes ISAM as an S1 run for cSoil was not available.
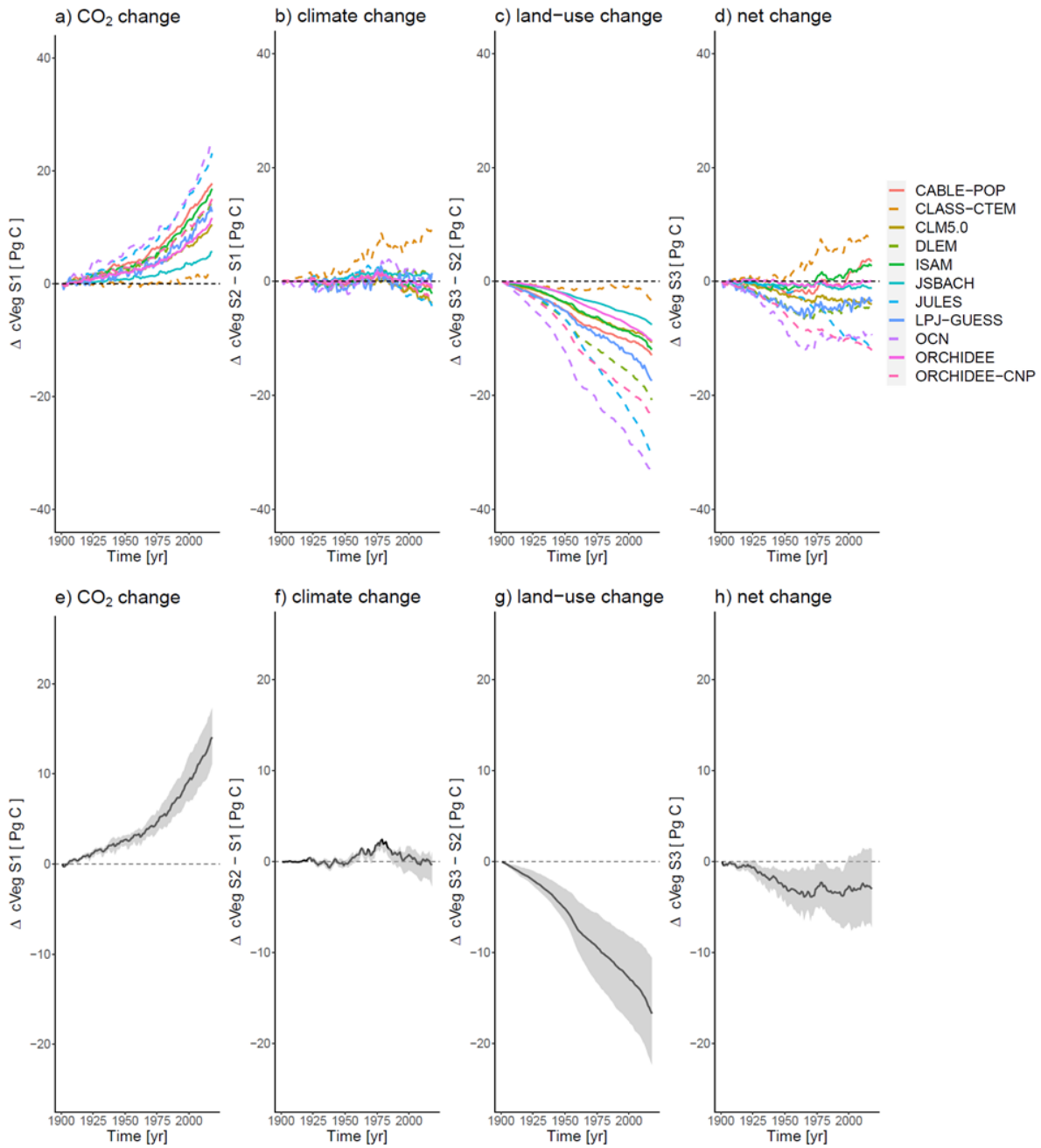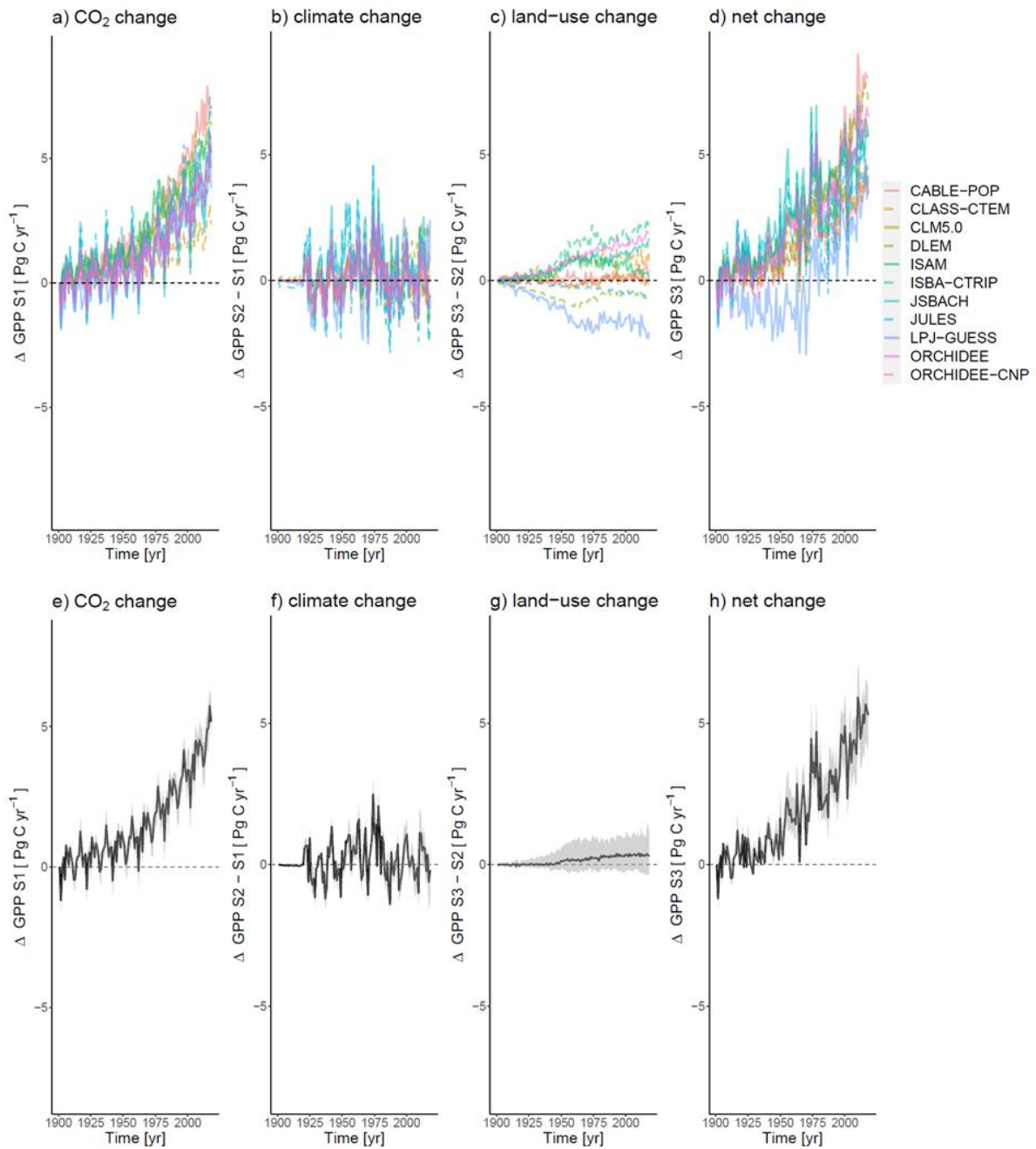
Fig. S16: Effects of a) CO2 increase, b) climate change, c) land-use change and d) combined GPP, using TRENDY model runs S1: changing CO2 and 20-yr recycled climatology, S2: changing CO2 and varying climatology and S3: changing CO2, varying climatology and land use change. (d-f) bold lines show model means with ribbons representing the interquartile range. The divergence is shown relative to 1901. The model set used to generate this figure excludes OCN as an S1 run for GPP was not available.

Fig. S17: Sensitivity analysis of extraction methods for comparing model outputs with different spatial resolution. Summed GPP pixel values at native model resolutions with different handling of border pixels. Contained: A pixel is only considered if it lies entirely within the boundary. Exact: The exact extent of the overlapping edge pixel is used. Extended: Any intersected pixel is considered in full.

Extracting values from rasters that have relatively coarse resolution can yield substantial differences due to the inclusion or exclusion of adjacent areas. Weighted extraction methods that account for partial coverage of cells within the boundary of a mask should be used when undertaking these kinds of analyses across datasets with two or more different native resolutions. Different methods could account for more than a 10-fold difference in the total productivity retrieved for drylands. When investigating the carbon dynamics of regions of variable spatial extents with strict boundaries, climatic or otherwise, the spatial resolutions at which LSMs are implemented must be considered appropriately when resampling.
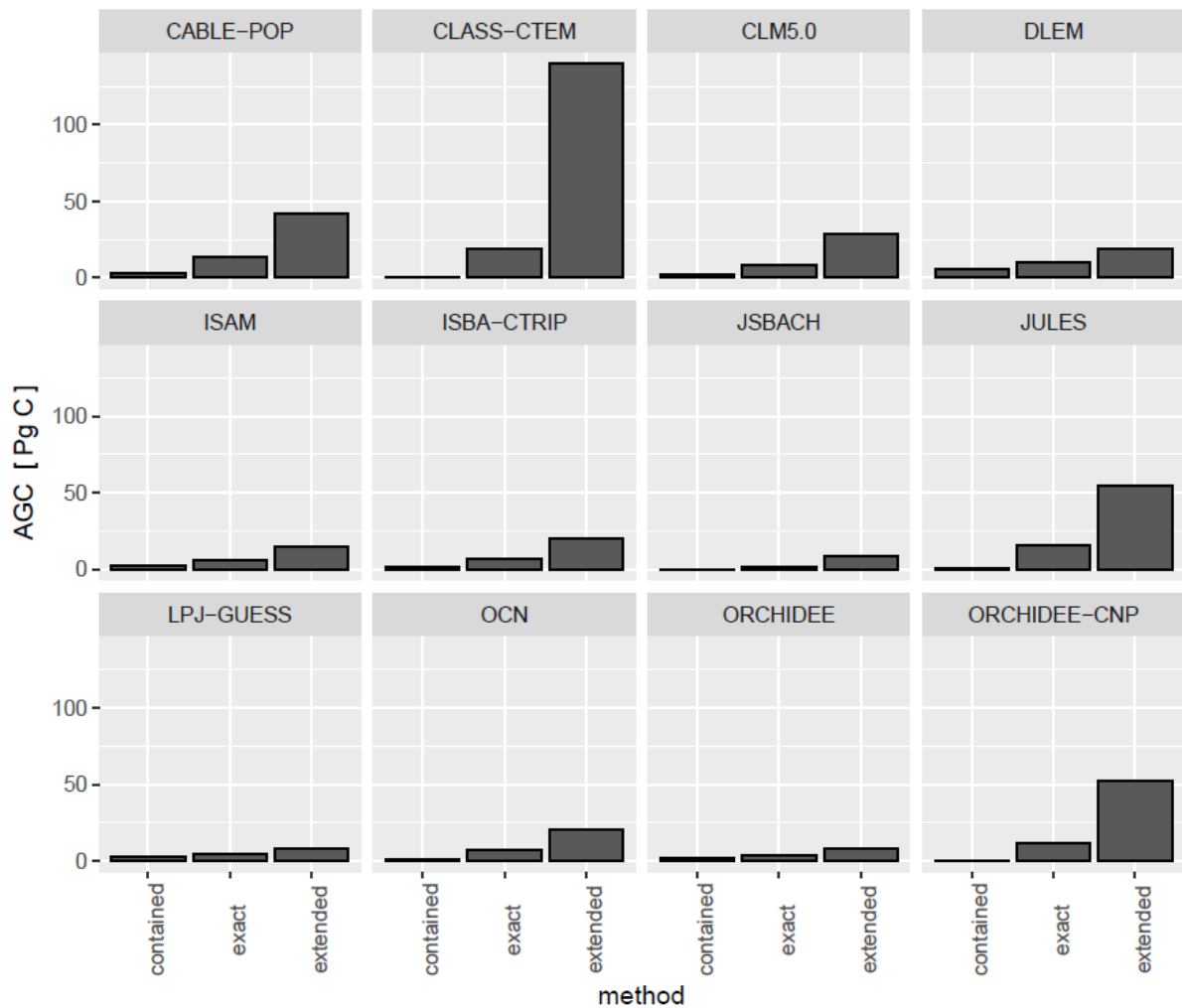
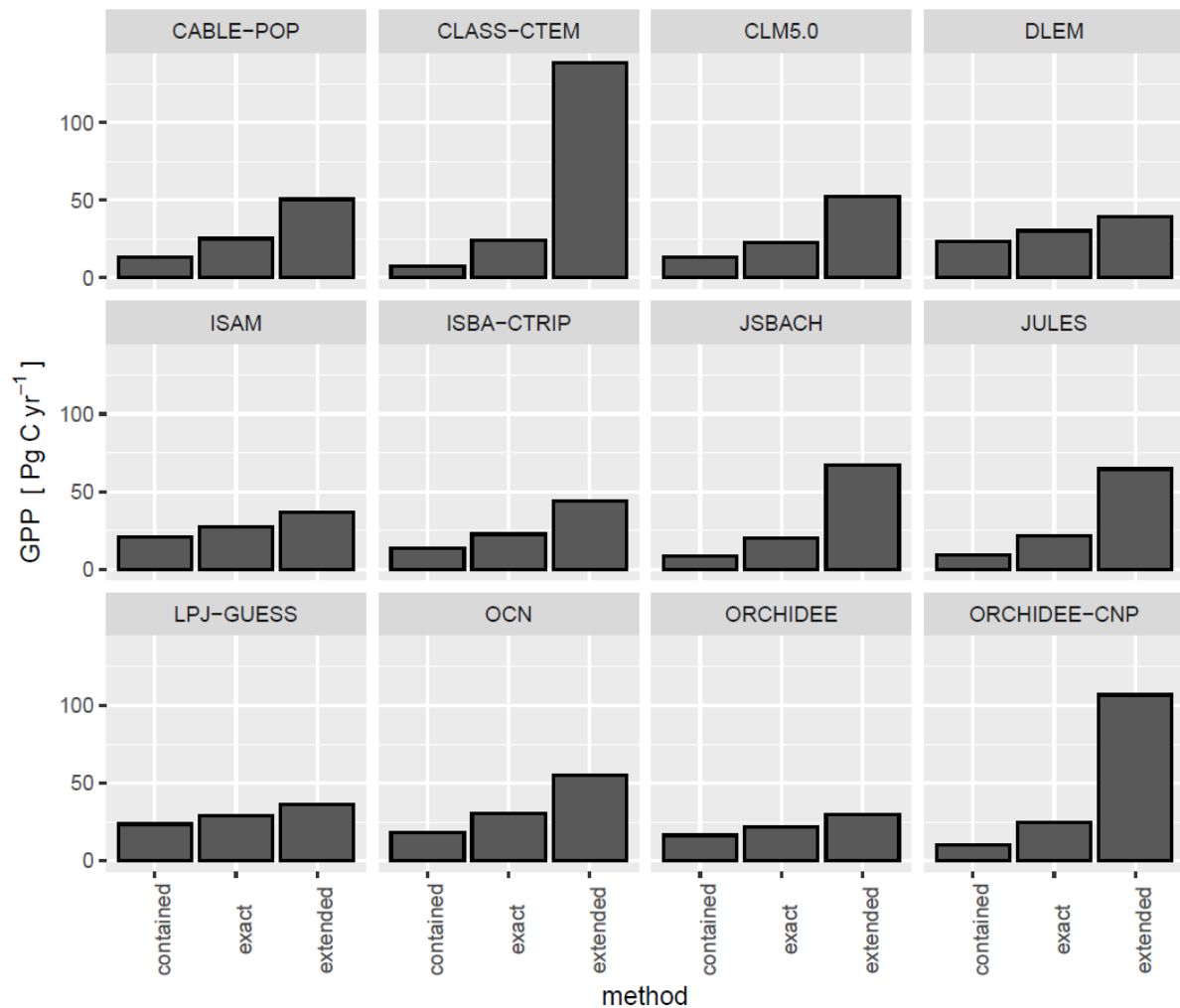Fig. S18: Sensitivity analysis of extraction methods for comparing model outputs with different spatial resolution. Summed AGC pixel values at native model resolutions with different handling of border pixels. Contained: A pixel is only considered if it lies entirely within the boundary. Exact: The exact extent of the overlapping edge pixel is used. Extended: Any intersected pixel is considered in full.

Extracting values from rasters that have relatively coarse resolution can yield substantial differences due to the inclusion or exclusion of adjacent areas. Weighted extraction methods that account for partial coverage of cells within the boundary of a mask should be used when undertaking these kinds of analyses across datasets with two or more different native resolutions. Different methods could account for more than a 10-fold difference in the total biomass retrieved for drylands. When investigating the carbon dynamics of regions of variable spatial extents with strict boundaries, climatic or otherwise, the spatial resolutions at which LSMs are implemented must be considered appropriately when resampling.
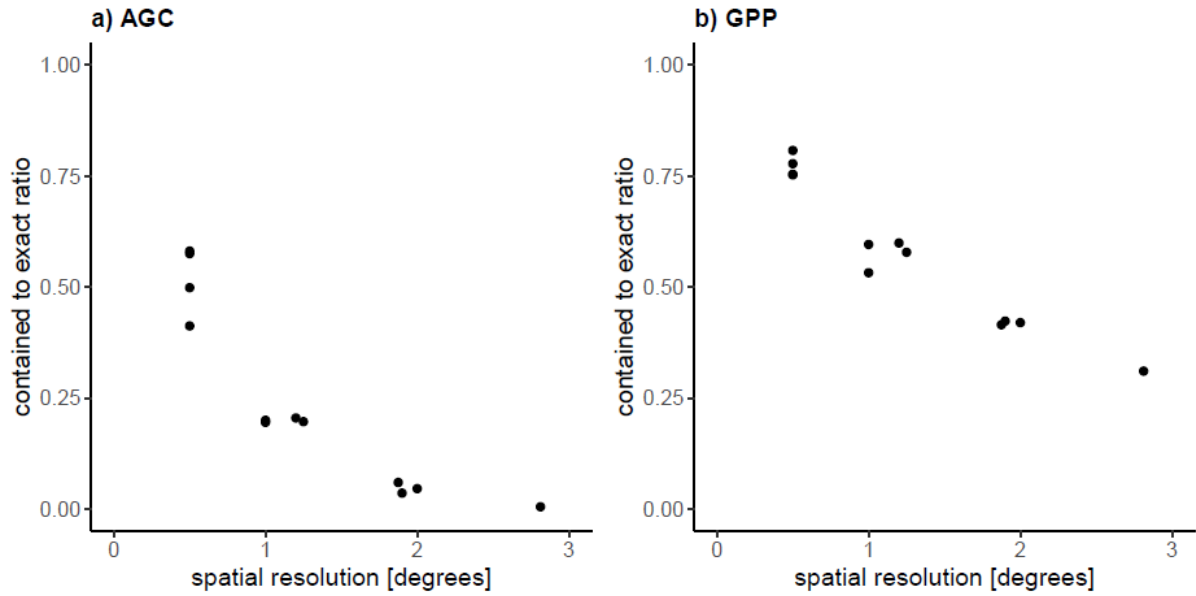
Fig. S19. Sensitivity analysis of extraction methods for comparing model outputs with different spatial resolution. The relative impact of different sampling approaches depends on grid resolution. On the y-axis are ratios of mean total a) cVeg and b) GPP values from using the contained grid-cell and exact methods respectively, the x-axis shows the model spatial resolution in degrees. The difference was more pronounced for coarser resolution datasets. When investigating the carbon dynamics of regions of variable spatial extents with strict boundaries, climatic or otherwise, the spatial resolutions at which LSMs are implemented must be considered appropriately when resampling.

Table S1. Global products used for analysis.

| Product | Type | Spatial resolution | Temporal resolution | Period | Reference |
|---------|------|--------------------|--------------------|--------|-----------|
| Productivity | PML-V2 (MODIS product) | 500 m | 8-day | 2000-02-26 to 2020-12-26 | (Zhang et al., 2019) |
| Biomass | L-VOD (vegetation optical depth) | 0.25° (approx. 25 km) | 3-day | 2010 to present | (Fernandez-Moran et al., 2017) |
| Precipitation Potential Evapotranspiration | TerraClimate | 2.5 arc minutes | monthly | 1958-2019 | (Abatzoglou et al., 2018) |
| Modelled GPP and Biomass | TRENDY (v8) S3 | 1° | GPP: monthly Biomass: yearly | 1901-2018 | (Friedlingstein et al., 2019) |
| Burned area | MCD64A1v006 (MODIS product) | 500 m | monthly | 2000 to present | (Giglio et al., 2015) |

Table S2: Pearson's r between different AGC maps resampled to 0.25° resolution and the filtered L-VOD values of the corresponding years. For AGC maps with reference year 2010, L-VOD for 2011 was used instead due to data availability.

| AGC product | Pearson's r |
|---|---|
| Globbiomass map (2010) | 0.76 |
| European Space Agency Climate Change Initiative Biomass map (2017) | 0.68 |
| Saatchi biomass map (2015) | 0.67 |
| Avitabile biomass map (2010) | 0.42 |

Table S3. A brief description of the 12 land surface models from TRENDY v8 that are included in this study.

| Model | Native spatial resolution | Dynamic natural land-cover changes | Ecosystem demography | Representation of Fire | Reference |
|-------|---------------------------|-----------------------------------|----------------------|----------------------|-----------|
| CABLE-POP | 1° × 1° | N | Y | N | (Haverd et al., 2018) |
| CLASS-CTEM | 2.8125° × 2.8125° | N | N | Y | (Melton & Arora, 2016) |
| CLM5.0 | 0.9375° × 1.25° | N | N | Y | (Lawrence et al., 2019) |
| DLEM | 0.5° × 0.5° | N | N | Y | (H. Tian et al., 2015) |
| ISAM | 0.5° × 0.5° | N | N | N | (Meiyappan et al., 2015) |
| ISBA-CTRIP | 1° × 1° | N | N | Y | (Delire et al., 2020) |
| JSBACH 3.2 | T63 (~1.9°) | N | N | Y | (Mauritsen et al., 2019; Reick et al., 2021) |
| JULES-ES-1.0 | 1.25° × 1.875° | Y | N | N | (Clark et al., 2011) |
| LPJ-GUESS | 0.5° × 0.5° | Y | Y | Y | (B. Smith et al., 2014) |
| OCN | 1° × 1.2° | N | N | N | (Zaehle & Friend, 2010) |
| ORCHIDEE | 0.5° × 0.5° | N | N | N | (Krinner et al., 2005) |
| ORCHIDEE-CNP | 2° × 2° | N | N | N | (Goll et al., 2017) |

Table S4. Slope parameters for linear models fitted to each time-series of GPP (global, 2001-2018) and AGC (four continents, 2011-2018) using robust Theil-Sen estimators. Grey shading indicates significant trends ($p < 0.05$).

| data | GPP slope | GPP p value | AGC slope | AGC p value |
|---|---|---|---|---|
| TRENDY mean | 0.122 | 0.003 | -0.017 | 0.174 |
| RS retrieved | -0.037 | 0.363 | -0.009 | 0.902 |
| CABLE-POP | 0.184 | 0.002 | 0.001 | 1.000 |
| CLASS-CTEM | 0.066 | 0.019 | 0.003 | 0.902 |
| CLM5.0 | 0.079 | 0.019 | -0.043 | 0.174 |
| DLEM | 0.131 | 0.001 | -0.022 | 0.266 |
| ISAM | 0.095 | 0.001 | -0.012 | 0.035 |
| ISBA-CTRIP | 0.111 | 0.002 | -0.006 | 0.174 |
| JSBACH | 0.118 | 0.015 | -0.008 | 0.009 |
| JULES | 0.078 | 0.005 | -0.062 | 0.001 |
| LPJ-GUESS | 0.159 | 0.000 | 0.014 | 0.902 |
| OCN | 0.132 | 0.058 | -0.022 | 0.386 |
| ORCHIDEE | 0.151 | 0.001 | -0.007 | 0.902 |
| ORCHIDEE-CNP | 0.082 | 0.001 | -0.033 | 0.004 |

Table S5: Mean total dryland C stocks and changes predicted by individual models (1901 to 2018) and deviation from the TRENDY mean value in 2018 in units of TRENDY models standard deviation, colours indicating over- (blue) and underestimation (red).

| model | cVeg mean | cSoil mean | cTotal mean | Δ cVeg | Δ cSoil | Δ cEco | cVeg deviation | cSoil deviation | cTotal deviation |
|---|---|---|---|---|---|---|---|---|---|
| CABLE.POP | 41.5 | 306.0 | 347.5 | 3.6 | 20.8 | 24.4 | 1.031 | 1.814 | 1.919 |
| CLASS.CTEM | 65.3 | 219.6 | 284.9 | 7.6 | -2.9 | 4.7 | 1.659 | -1.158 | 0.124 |
| CLM5.0 | 30.9 | 213.5 | 244.4 | -4.0 | 11.1 | 7.1 | -0.165 | 0.596 | 0.337 |
| DLEM | 54.4 | 168.3 | 222.7 | -5.0 | -6.2 | -11.2 | -0.315 | -1.571 | -1.325 |
| ISAM | 56.9 | 239.5 | 296.4 | 2.7 | 7.4 | 10.2 | 0.895 | 0.137 | 0.621 |
| JSBACH | 11.5 | 90.7 | 102.3 | -1.2 | 9.7 | 8.5 | 0.279 | 0.417 | 0.466 |
| JULES | 84.8 | 381.4 | 466.3 | -11.8 | 9.7 | -2.2 | -1.385 | 0.414 | -0.506 |
| LPJ.GUESS | 25.7 | 373.0 | 398.7 | -3.2 | -0.4 | -3.6 | -0.037 | -0.846 | -0.637 |
| OCN | 43.6 | 470.5 | 514.1 | -9.4 | 6.1 | -3.3 | -1.008 | -0.026 | -0.605 |
| ORCHIDEE | 20.3 | 112.8 | 133.1 | 0.0 | 14.0 | 14.0 | 0.468 | 0.960 | 0.970 |
| ORCHIDEE.CNP | 70.1 | 155.0 | 225.0 | -12.1 | 0.5 | -11.6 | -1.423 | -0.737 | -1.364 |